Manuscript prepared for Atmos. Chem. Phys.
with version 2014/07/09 7.01 Copernicus papers of the LaTeX class copernicus.cls.
Date: 17 August 2014

Solar cycle in current reanalyses: (non)linear attribution study

Ales Kuchar[1], **Petr Sacha**[1], **Jiri Miksovsky**[1], **and Petr Pisoft**[1]

[1]The Department of Meteorology and Environment Protection, Charles University in Prague, V Holesovickach 2, 180 00 Prague 8, Czech Republic

Correspondence to: A. Kuchar (kuchara@mbox.troja.mff.cuni.cz)

Abstract. This study is focused on the variability of temperature, ozone and circulation characteristics in the stratosphere and lower mesosphere with regard to the influence of the eleven-year solar cycle. It is based on the attribution analysis using multiple nonlinear techniques (Support Vector Regression, Neural Networks) besides traditional linear approach. The analysis was applied for the 1979-2013 period on several current reanalysis datasets, including MERRA, ERA-Interim and JRA-55, with the aim to compare how this type of data resolves especially the double-peaked solar response in the temperature and ozone variables and consequent changes induced by these anomalies. Equatorial temperature signals in the lower and upper stratosphere were found sufficiently robust and they are in qualitative agreement with previous observational studies. The analysis also pointed to the solar signal in the ozone datasets (i.e. MERRA and ERA-Interim) not being consistent with the observed double-peaked ozone anomaly extracted from satellite measurements. Consequently the results obtained by the linear regression were confirmed by the nonlinear approach through all datasets, suggesting that linear regression is a relevant tool to sufficiently resolve the solar signal in the middle atmosphere. Furthermore, the seasonally dependence of the solar response was also discussed, mainly as a source of dynamical causalities in the waves propagation characteristics in the zonal wind and the induced meridional circulation in the winter hemispheres. The hypothetical mechanism of weaker Brewer Dobson circulation was reviewed together with discussion of the polar vortex stability.

1 Introduction

The Sun is a prime driver of various processes in the climate system. From observations of Sun's variability on decadal or centennial time scales, it is possible to identify the temporal patterns and trends of the solar activity, and consequently to derive the related mechanisms of the solar influence on the Earth's climate (e.g. Gray et al., 2010). Of the semi-regular solar cycles, the most prominent is the approximately eleven years periodicity which manifests in the solar magnetic field or through fluctuations of sunspot number, but also in the total solar irradiance (TSI) or the solar wind properties. For the dynamics of the middle atmosphere, where the ozone production and destruction occur, the changes in the spectral irradiance are the most influential, since the TSI as the integral over all wavelengths exhibits variations of orders lower than the ultraviolet part of spectrum (Lean, 2001). This fact was supported by original studies (e.g. Labitzke, 1987; Haigh, 1994) that suggested the solar cycle influence on the variability of the stratosphere. Gray et al. (2009) have shown by the fixed dynamical heating model that response of the temperature in the photochemically controlled region of the upper stratosphere is given approximately in 60% by direct solar heating and in 40% due to indirect effect by the ozone changes.

Numerous observational studies identified temperature and ozone changes linked to the eleven year cycle by multiple linear regression. Using ERA-40 reanalysis, Frame and Gray (2010) pointed to a manifestation of annually averaged solar signal in temperature, exhibiting predominantly around equator with amplitudes up to 2 K around stratopause and with a secondary amplitude maximum up to 1 K in the lower stratosphere. Soukharev and Hood (2006), Hood et al. (2010) and Randel and Wu (2007) have used satellite ozone data sets to characterize statistically significant responses in the upper and lower stratosphere. Observed double-peaked ozone anomaly in the vertical profile around equator was confirmed by the simulations of coupled chemistry climate models (**?**).

Statistical studies (e.g. Labitzke et al., 2006; Camp and Tung, 2007) have also focused on the lower stratospheric solar signal in the polar regions and revealed modulation by the Quasi-biennial oscillation (QBO), or the well known Holton-Tan relationship (Holton and Tan, 1980) modulated by the

solar cycle. Proposed mechanisms suggested that the solar signal induced during early winter in the upper equatorial stratosphere propagates poleward and downward when the stratosphere transits from radiatively controlled state to the dynamically controlled state involving the planetary wave propagation (Kodera and Kuroda, 2002). The mechanism of the solar cycle and QBO interaction which roots from reinforcing each other or canceling each other out (Gray et al., 2004) has been verified by recent model simulations (Matthes et al., 2013). Those proved independence of the solar response in the tropical upper stratosphere and the response depending on the presence of the QBO in lower altitudes.

The ozone and temperature perturbations associated with the solar cycle have impact on the middle atmospheric circulation. They produce zonal wind anomaly around stratopause (faster subtropical jet) during the solar maxima through the enhanced meridional temperature gradient. Since the planetary wave propagation is affected by the zonal mean flow (Andrews and McIntyre, 1987), we can suppose that the stronger subtropical jet can deflect planetary waves propagating from higher latitudes. Reduced wave forcing can lead to decreasing/increasing upwelling/downwelling motions in the equatorial, or higher latitudes respectively (Kodera and Kuroda, 2002). The Brewer-Dobson circulation (BDC) is weaker during the solar maxima (Gray et al., 2010) although this appears to be sensitive to state of the polar winter. Observational studies together with model experiments (e.g. Matthes et al., 2006) suggest a so-called "Top-Down" mechanism when the solar signal is transferred from the upper to lower stratosphere, and even to the tropospheric altitudes.

Observational and modeling studies over the past two decades have fundamentally changed our understanding of wave processes and coupling between the middle atmosphere and tropospheric conditions (Gerber et al., 2012). It was shown that stratosphere plays significant and active role in the tropospheric circulation on various time scales (Baldwin and Dunkerton, 1999; Lu et al., 2013; Solomon et al., 2010). Deeper understanding of the mechanisms of communication between middle atmosphere and troposphere contributes to better climate change predictions. However, a number of questions about the coupling processes with regard to the solar signal perturbation have to be answered. It has been shown that difficulties of the state-of-the-art climate models arise when reproducing the solar signal influence on the winter polar circulation, especially in less active sun periods (Ineson et al., 2011). The hypothesis is that the solar UV forcing is too weak in the models. Satellite measurements indicate that variations in the solar UV irradiance may be larger than was previously thought (Harder et al., 2009).

At the Earth's surface, the detection of the solar cycle influence is problematic since there are other significant forcings factors, i.e. greenhouse gases, volcanoes and aerosols changes (Gray et al., 2010), as well as substantial variability attributable to internal climate dynamics. However several studies (van Loon et al., 2007; van Loon and Meehl, 2008; Hood and Soukharev, 2012; Hood et al., 2013; Gray et al., 2013) detected the solar signal in the sea level pressure or sea surface temperature which support hypothesis of a troposphere-ocean response to the solar cycle. The studies (e.g. Hood and Soukharev, 2012) suggest a so-called "Bottom-Up" solar forcing mechanism. That contributes to the lower ozone and temperature anomaly in connection with the lower stratosphere deceleration of the BDC.

Several past studies (e.g. Soukharev and Hood, 2006; Frame and Gray, 2010; Gray et al., 2013) used multiple linear regression technique to extract the solar signal and separate other climate phenomena like the QBO, aerosol's effect, NAO, ENSO or trend variability. Except for this conventional method, it is possible to use alternative approaches to isolate and examine particular signal components, such as wavelet analysis (Pisoft et al., 2012, 2013) or empirical mode decomposition (Coughlin and Tung, 2004). Nonlinear character of the climate system also suggests potential benefits from application of alternative, full nonlinear attribution techniques for study of properties and interactions in the atmosphere. However, such nonlinear techniques have been used rather sporadically in the atmospheric sciences (e.g. Walter and Schönwiese, 2003; Pasini et al., 2006; Blume and Matthes, 2012), mainly due to their several disadvantages like the lack of explanatory power (Olden and Jackson, 2002).

To examine the middle atmospheric conditions, it is necessary to study reliable and sufficiently vertically resolved data. Systematic and global observations of the middle atmosphere only began during the International Geophysical Year (1957-1958) and were later expanded by development of the satellite measurements (Andrews and McIntyre, 1987). Supplementary data come from the balloon and rocket soundings, though these are limited by their vertical range (only lower stratosphere in case of radiosondes) and the fact that the in situ observations measure local profiles only. By assimilation of these irregularly distributed data and discontinuous measurements of particular satellite missions into an atmospheric/climatic model, we have available modern basic datasets for climate research, so called reanalyses. These types of data are relatively long, globally gridded with vertical range to upper stratosphere or the lower mesosphere and thus suitable for the 11-yr solar cycle research. In spite of their known limitations (discontinuities in ERA reanalysis McLandress et al., 2013), they are considered an extremely valuable research tool (Rienecker et al., 2011). Coordinated intercomparison is initiated by SPARC community to understand current reanalysis products, and to contribute to future reanalysis improvements (Fujiwara et al., 2012).

2 Datasets

Our analysis was applied on the last generation of three reanalyzed datasets: MERRA (Modern Era Reanalysis for

Research and Applications, developed by NASA) (Rienecker et al., 2011), ERA-Interim (ECMWF Interim Reanalysis) (Dee et al., 2011) and JRA-55 (Japanese 55-year Reanalysis) (Ebita et al., 2011). We have studied series for the 1979-2013 time period. All of the datasets were analyzed on the monthly basis. The Eliassen-Palm (EP) flux diagnostics (described below) was analysed on the daily basis and subsequently the monthly means were produced. The vertical range extends to the lower mesosphere (0.1 hPa) for MERRA, and to 1 hPa for remaining ones. The horizontal resolution of the gridded datasets was $1.25°$x$1.25°$ for MERRA and JRA-55 and $1.5°$x$1.5°$ for ERA-Interim respectively.

In comparison with previous generation of reanalyses, it is possible to observe better representation of stratospheric conditions. This improvement is considered to be connected with increasing the height of upper boundary of model domain (Rienecker et al., 2011). The Brewer-Dobson circulation was markedly overestimated by ERA-40, an improvement was achieved in ERA-Interim, but the upward transport remains faster than observations indicate (Dee et al., 2011). Interim results of JRA-55 suggest less biased reanalyzed temperature in the lower stratosphere relative to JRA-25 (Ebita et al., 2011).

Except for the standard variables provided in reanalysis, i.e. air temperature, ozone mixing ratio and circulation characteristics – zonal, meridional or omega velocity, we have also analyzed other dynamical variables. Of particular interest was the EP flux diagnostics - a theoretical framework to study interactions between planetary waves and the zonal mean flow (Andrews and McIntyre, 1987). Furthermore, this framework allows studying the waves propagation characteristics in the zonal wind and the induced (large scale) meridional circulation as well. For this purpose the quasi-geostrophic approximation of Transformed Eulerian Mean (TEM) equations was used, in the form employed by (Edmon Jr et al., 1980).

3 Methods

To detect variability and changes due to external climate factors, such as the eleven year solar cycle, we have applied an attribution analysis based on the multiple linear regression and two nonlinear techniques. Regression model separates effects of climate phenomena that are supposed to have impact on the middle atmospheric conditions. Our regression model of particular variable X is described by the following equation:

$$
\begin{aligned}
X(t,z,\varphi,\lambda) &= \sum_{i=1}^{12} \alpha_i(z,\varphi,\lambda) + \beta(z,\varphi,\lambda)\,\mathbf{t} \\
&+ \boxed{\gamma(z,\varphi,\lambda)\,\mathbf{SOLAR}(t)} + \delta_1(z,\varphi,\lambda)\,\mathbf{QBO_1}(t) \\
&+ \delta_2(z,\varphi,\lambda)\,\mathbf{QBO_2}(t) + \delta_3(z,\varphi,\lambda)\,\mathbf{QBO_3}(t) \\
&+ \epsilon(z,\varphi,\lambda)\,\mathbf{ENSO}(t) + \zeta(z,\varphi,\lambda)\,\mathbf{SAOD}(t) \\
&+ \eta(z,\varphi,\lambda)\,\mathbf{NAO}(t) + \mathbf{e}(t,z,\varphi,\lambda). \quad (1)
\end{aligned}
$$

After deseasonalizing that can be represented by α_i indices we have applied trend regressor t either in the linear form or with inclusion of the Equivalent Effective Stratospheric Chlorine (EESC) index (that should be employed due to ozone trend turnover around middle of the nineties). The solar cycle is represented by the 10.7 cm radio flux as a proxy which correlates well with the sunspot number variation (the data were acquired from Dominion Radio Astrophysical Observatory (DRAO) in Penticton, Canada).

We have included the quasi-biennial proxies as another stratosphere-related predictor. Similar studies have represented the QBO in the multiple regression methods in several ways. Our approach involves three separate QBO indices extracted from the MERRA reanalysis. These three indices are the first three principal components of the residuals of our linear regression model (1) excluding QBO predictors applied to the equatorial zonal wind. The approach follows paper by Frame and Gray (2010), or study (Crooks and Gray, 2005). The three principal components explain 49%, 47% and 3% of the total variance. The extraction of the first two components reveals 28 months periodicity and out-of phase relationship between the upper and lower stratosphere. Out-of phase relationship or orthogonality manifests by approximately quarter period shift of these components. Deviation from the QBO quasi-regular period represented by the first two dominant components is contained in the residual variance of 4%. The linear regression analysis of the zonal wind with inclusion of the first two principal components reveals statistically significant linkage between the third principal component and the residuals of this analysis. Furthermore, the regression coefficient of this QBO proxy was statistically significant for all variables tested at p-value < 0.05 (see below for details about statistical significance techniques). Wavelet analysis demonstrates three statistically significant but non-stationary periods exceeding the level of white noise wavelet spectrum (not shown): approximately annual cycle (peak period of 1 year and 2 months), cycle with the peak period of 3 year and 3 months and long-period cycle (peak period between 10 and 15 years). Those interferences can be attributed to the possible non-linear interactions between the QBO itself and other signals like the annual cycle or long-period cycle such as the eleven year solar cycle at the equatorial stratosphere.

El Niño Southern Oscillation (ENSO) is represented by the Multivariate ENSO index (MEI) which is computed as the first principal component of the six main observed variables over the Pacific ocean: sea level pressure, zonal and meridional wind, sea surface temperature, surface air temperature and total cloudiness fraction of the sky (NCAR, 2013). Effect of volcanic eruptions is represented by the Stratospheric Aerosol Optical Depth (SAOD). The time series was derived from the optical extinction data (Sato et al., 1993). We have used globally averaged time series in our regression model. The North Atlantic Oscillation (NAO) has been also included with the respective index derived by rotated principal component analysis technique applied on the monthly standardized 500-hPa height anomalies obtained from the Climate Data Assimilation System (CDAS) in the Atlantic region between 20°N-90°N (NWS, 2013).

The multiple regression model via eq. (1) has been used for the attribution analysis, and supplemented by two nonlinear techniques. The linear approach is based on estimating regression coefficients by Multiple Linear Regression (MLR) method. To avoid the effect of autocorrelation of residuals and to obtain Best Linear Unbiased Estimate (BLUE) according to the Gauss-Markov theorem (Thejll, 2005), we have used iterative algorithm to model the residuals as a second-order autoregressive process. The Durbin-Watson statistic has been used to detect autocorrelation of the error terms from the regression model. As a result of the uncorrelated residuals, we can suppose the standard deviations of the estimated regression coefficients not to be diminished (Neter et al., 2004). The statistical significance of regression coefficients was computed by the t-test and verified by bootstrap significance test.

The nonlinear approach consisted of the Multi Layer Perceptron (MLP) and relatively novel Suppport Vector Regression (SVR) technique in our case. The MLP as a technique inspired by human brain is highly complex and capable of capturing non-linear interactions between inputs (regressors) and output (modelled data) (e.g. Haykin et al., 2009). Nonlinear approach is achieved by transferring the input signals through a sigmoid function in a particular neuron and within a hidden layer propagating to the output (so called feedforward propagation). The standard error backpropagation iterative algorithm to minimize the global error has been used.

The Support Vector Regression technique belongs to category of kernel methods. Input variables were nonlinearly transformed to a high-dimensional space by radial basis (Gaussian) kernel, where a linear classification (regression) can be constructed (Cortes and Vapnik, 1995). However, crossvalidation must be used to establish kernel parameter and cost function. We have used 5-fold crossvalidation to optimize the SVR model selection for every point in the dataset as a trade-off between the recommended number of folds (Kohavi et al., 1995) and computational time. The MLP model was validated by holdout method since this method is in order of magnitude more expensive to computational time. The datasets was separated into the training set (75% of whole dataset) and the testing set (25% of whole dataset).

The earlier mentioned lack of the explanatory power of the nonlinear techniques comes mainly from nonlinear interactions during signal propagation and the impossibility of directly monitoring the influence of the input variables. In contrast to the linear regression approach, the understanding of relationships between variables is quite problematic. For this reason, responses of our variables have been modelled by a technique originating from the sensitivity analysis and used by e.g. Blume and Matthes (2012). The relative impact RI of each variable was computed as

$$RI = \frac{I_k}{\sum I_k}, \tag{2}$$

where $I_k = \sigma(\hat{y} - \hat{y_k})$. $\hat{y}$ and $\hat{y_k}$ is original model output and model output when k-input variable was held on their constant level respectively. There are a lot of possibilities which constant level to choose. It is possible to choose several levels and then to observe sensitivity of model outputs varying for example on minimum, median and maximum levels. Our sensitivity measure (relative impact) was based on the median level. The primary reason comes from pure practical considerations - to compute our results fast enough as another weakness of the nonlinear techniques consists in a larger requirement on computational capacity. In general this approach was chosen because of their relative simplicity of comparing all techniques to each other and to be able to interpret them too. The contribution of variables in neural network models has been already studied and Gevrey et al. (2003) brought review and comparison of these methods.

4 Results

4.1 Annual response (MERRA)

Figure 1 shows the annually averaged solar signal in the zonal and altitudinal means of temperature, zonal wind, geopotential height and ozone mixing ratio. The signal is expressed as the average difference between the solar maxima and minima in the 1979-2013 period. Statistically significant responses detected by the linear regression in the temperature series (see Fig. 1(a)) are positive and are located around the equator in the lower stratosphere with values of about 0.5°C. The temperature response increases to 1°C in the upper stratosphere at the equator and up to 2°C at the poles. The significant solar signal anomalies are more variable around the stratopause and not limited to the equatorial regions. Hemispheric asymmetry of the statistical significance can be observed in the lower mesosphere. From relative impact point of view (in Figs. 1(b)-(d) marked as RI), it is difficult to detect signal with the impact larger than 20% in the lower stratosphere where the volcanic and QBO impacts dominate. In the upper layers (where the solar signal

expressed by the regression coefficient is continuous across the equator) we have detected relatively isolated signals (over 20%) around $\pm 15^{\circ}$ using the relative impact method. The hemispheric asymmetry manifests also in the relative impact field, especially in the SVR field in the mesosphere.

The annually averaged solar signal in the zonal-mean of zonal wind (Figs. 1(e)-(h)) dominates around the stratopause as an enhanced subtropical westerly jet. The zonal wind variability due to the solar cycle corresponds with the temperature variability due to the change of the meridional temperature gradient and via the thermal wind equation. The largest positive anomaly in the northern hemisphere reaches 4 m/s around 60 km (shown in Fig. 1(e)). In the southern hemisphere, the anomaly is smaller and not statistically significant. There is a significant negative signal in the southern polar region and also at the equator especially in the mesosphere. The negative anomalies correspond with weakening of the westerlies or amplification of the easterlies. The relative impact of the solar cycle is located zonally similarly even for both nonlinear techniques (Figs. 1(f)-(h)). The equatorial region across all the stratospheric layers is influenced dominantly by the QBO (expressed by all 3 QBO regressors) and for this reason the solar impact is minimized around the equator.

The pattern of the solar response in geopotential height (Figs. 1(i)-(l)) shows positive values in the upper stratosphere and lower mesosphere. That is also consistent with the zonal wind field thorough thermal wind balance. In the geopotential field, the solar cycle influences the most extensive area among all regressors. The impact area includes almost whole mesosphere and the upper stratosphere.

Last row of Fig. 1 also shows the annual mean solar signal in the zonal mean of the ozone mixing ratio (expressed as percent change from the solar maximum to the solar minimum). Using the model with EESC instead of linear trend over whole period, we tried to capture the ozone trend change around the year 1996. Another possibility was using our model over two individual periods, e.g. 1979-1995 and 1996-2013, but the results were quantitatively similar. The main common feature with other results is the positive ozone response in the lower stratosphere, ranging from 1 to 3 percent change. The majority of results share the positive ozone response. In the equatorial upper stratosphere, no other relevant solar signal was detected compared to study based on satellite measurement (Soukharev and Hood, 2006). By the relative impact method (Figs. 1(n)-(p)), we have obtained results comparable with linear regression coefficients, but especially around stratopause the impact suggested by nonlinear techniques does not reach the values achieved by the linear regression.

4.1.1 Annual response (comparison with JRA-55, ERA-Interim)

Comparison of the results for the MERRA and JRA-55 temperature, zonal wind and geopotential height shows that the annual responses to the solar signal are in a qualitative agreement (compare Figs. 1, 2 and 3). The zonal wind and geopotential response seems to be consistent in all presented methods and datasets. The largest discrepancies can be seen in the upper stratosphere and especially in the temperature field (first row in these figures). The upper stratospheric equatorial anomaly was not detected by any of the regression techniques in case of the JRA-55 reanalysis. On the other hand, the anomaly in the ERA-Interim temperature in Fig. 2 reaches almost the same value as in the MERRA series.

The variability of the solar signal in the MERRA stratospheric ozone series was compared with the ERA-Interim results. The analysis points to large differences in the ozone response to the solar cycle between the reanalyses and even in comparison with satellite measurements by Soukharev and Hood (2006). In comparison with the satellite measurements, no relevant solar signal was detected in the upper stratosphere in the MERRA series. The signal seems to be shifted above the stratopause (confirmed by all techniques, shown in Figs. 1 and 2 (m)-(p)). Regarding the ERA-Interim, there is an ozone response to the solar cycle in the upper stratosphere. This statistically significant response indicates negative anomalies with values reaching up to 2% above the equator and up to 5% in the polar regions of both hemispheres. The negative response can be connected with a higher destruction of ozone during the solar maximum period and consequent heating of the region. Lower stratospheric solar signal in the ERA-interim is not limited to the equatorial belt $\pm 30^{\circ}$ up to 20 hPa like in the case of the MERRA reanalysis, and the statistical significance of this signal is rather reduced. The solar signal is detected higher and extends from the subtropical areas to the polar regions. The results suggest that the solar response in the MERRA series is more similar to the results from satellite measurements (Soukharev and Hood, 2006). Nevertheless, further comparison with independent data sets is needed to asses the data quality in detail.

4.1.2 Comparison of the linear and nonlinear approaches (MLR vs. SVR & MLP)

In this paper, we have applied and compared one linear (MLR) and two nonlinear attribution (SVR and MLP) techniques. The response of the studied variables to the solar signal and other forcings was studied using the sensitivity analysis approach (Blume and Matthes, 2012). This approach does not recognize positive or negative response as the linear regression does. For this reason, the relative impact results are compared to the regression's coefficients. Using the linear regression, it would be possible to analyze the statistical sig-

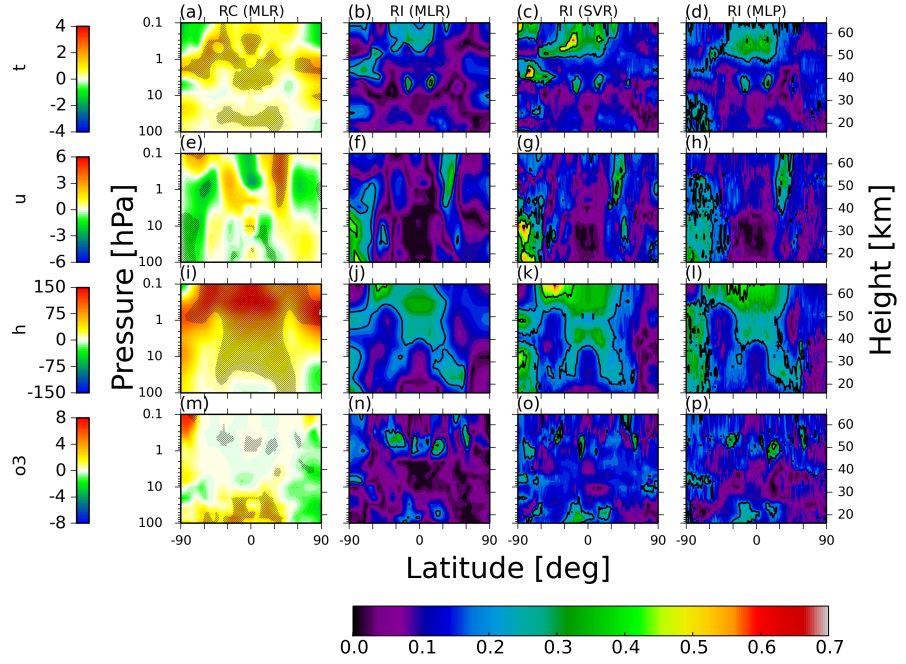

Figure 1. The annually averaged response of solar signal in the MERRA zonal-mean temperature t (a)-(d), unit: $[^{\circ}\mathrm{C}]$; zonal wind u (e)-(h), unit: $[\mathrm{m/s}]$; geopotential height h (i)-(l), unit: $[\mathrm{m}]$; and ozone mixing ratio $o3$ (m)-(p), unit: percentage change per annual mean. The response is expressed as regression coefficient RC (corresponding units per S_{max} minus S_{min}) in the left column and relative impact RI approach in the remaining columns. The relative impact was modeled by MLR, SVR a MLP techniques. The black contour levels in RI plots are 0.2, 0.4, 0.8 and 1.0. Statistical significance of scalar fields was computed by t-test. Hatches indicates p-values < 0.05.

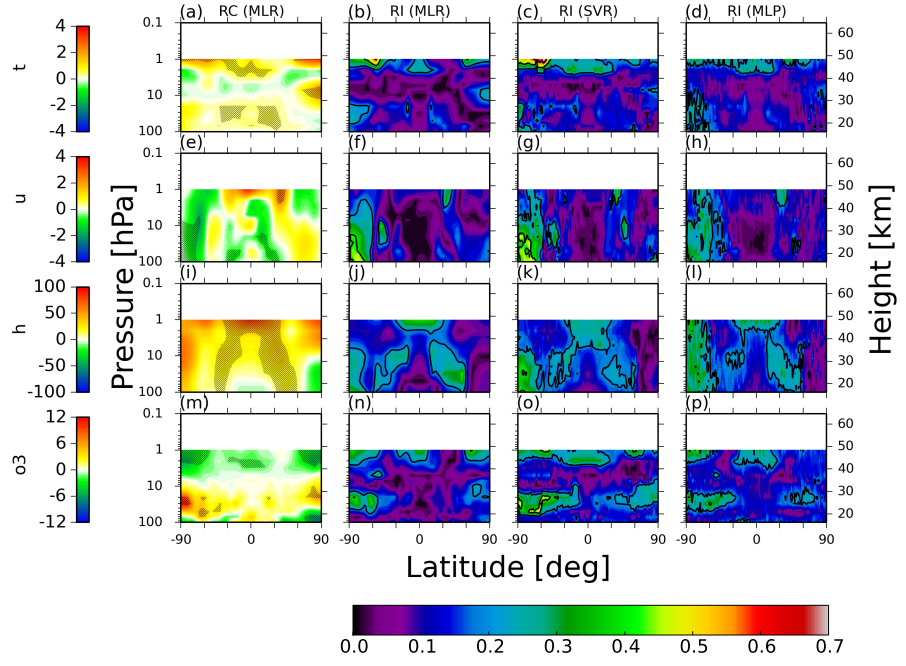

Figure 2. The annually averaged response of solar signal in the ERA-Interim zonal-mean temperature t (a)-(d), unit: $[^{\circ}\mathrm{C}]$; zonal wind u (e)-(h), unit: $[\mathrm{m/s}]$; geopotential height h (i)-(l), unit: $[\mathrm{m}]$; and ozone mixing ratio $o3$ (m)-(p), unit: percentage change per annual mean. The response is expressed as regression coefficient RC (corresponding units per S_{max} minus S_{min}) in the left column and relative impact RI approach in the remaining columns. The relative impact was modeled by MLR, SVR a MLP techniques. The black contour levels in RI plots are 0.2, 0.4, 0.8 and 1.0. Statistical significance of scalar fields was computed by t-test. Hatches indicates p-values < 0.05.

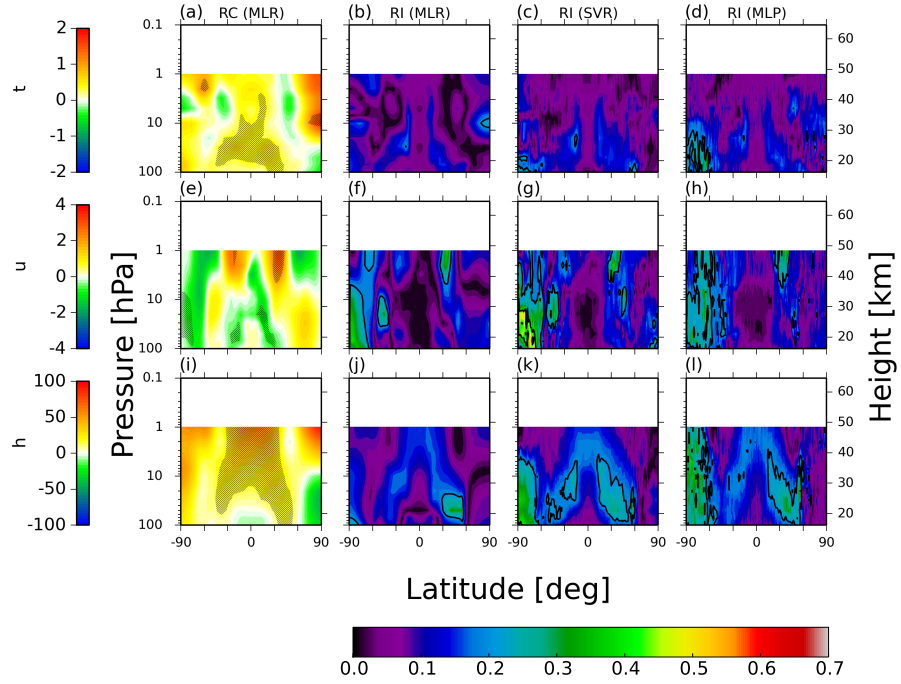

Figure 3. The annually averaged response of solar signal in the JRA-55 zonal-mean temperature t (a)-(d), unit: $[^{\circ}\mathrm{C}]$; zonal wind u (e)-(h), unit: $[\mathrm{m/s}]$; geopotential height h (i)-(l), unit: $[\mathrm{m}]$; and ozone mixing ratio $o3$ (m)-(p), unit: percentage change per annual mean. The response is expressed as regression coefficient RC (corresponding units per S_{max} minus S_{min}) in the left column and relative impact RI approach in the remaining columns. The relative impact was modeled by MLR, SVR a MLP techniques. The black contour levels in RI plots are 0.2, 0.4, 0.8 and 1.0. Statistical significance of scalar fields was computed by t-test. Hatches indicates p-values < 0.05.

nificance of the regression's coefficients and particular level of the relative impact. Due to higher variance, the significance levels of the relative impact are not estimated. Comparison between the linear and nonlinear approaches by the relative impact fields shows qualitative and in most regions also quantitative agreement. The most pronounced agreement is observed in the zonal wind (Figs. 1, 2 and 3(f)-(h)) and geopotential height fields (Figs. 1, 2 and 3(j)-(l)) . On the other hand the worst agreement is captured in the ozone field where nonlinear techniques have a problem to identify the upper stratospheric ozone anomaly detected by linear regression, although the lower stratospheric ozone anomaly is represented similarly by all techniques. In the temperature field the upper stratospheric solar signal reaches values over 20%, some individual signals in the northern hemisphere reach even 40%. However, using the relative impact approach, the lower stratospheric solar signal in the temperature field (that is well established by the regression coefficient) does not reach even 20% because of the QBO and volcanic effects dominance there. These facts emphasize that nonlinear techniques contribute to a robustness of the attribution analysis since the linear regression results were plausibly confirmed by the SVR and MLP techniques.

However, the statistical significance of individual response could have been estimated by bootstrap technique, which is quite expensive for the computational time, and for this reason was not applied. The comparison of various statistical approaches (MLR, SVR and MLP) should actually contribute to a robustness of the attribution analysis including the statistically assessed uncertainties. These uncertainties could partially stem from the fact that the SVR and Neural networks techniques are dependent on optimal model setting which is based on rigorous crossvalidation process, which places high demands on computing time.

The major differences between the techniques can be seen in the way of how they can simulate the original time series, i.e. coefficient of determination. For instance, the differences of the explained variance reach up to 10% between linear and nonlinear techniques, although the structure of coefficient of determination is almost the same. To conclude, nonlinear techniques show an ability to simulate the middle atmosphere variability with higher accuracy than crossvalidated linear regression .

4.2 Monthly response (MERRA)

As was pointed out by Frame and Gray (2010), it is necessary to examine the solar signal in individual months because of variable solar impact throughout the year. For example, the amplitude of the lower stratospheric solar signal in the northern polar latitudes in February exceeds the annual response since the solar cycle influence on vortex stability

is pronounced most in February. Besides the radiative influences of the solar cycle, we discuss the dynamical response throughout polar winter (Kodera and Kuroda, 2002).

Statistically significant upper stratospheric equatorial anomalies in the temperature series (winter months in Figs. 4 and 5(a)-(d)) are expressed in almost all months. Their amplitude and statistical significance vary throughout the year. The variation between the solar maxima and minima could be up to 1°C in some months. Outside the equatorial regions, the fluctuation could reach several °C. The lower stratospheric equatorial anomaly strengthens during winter. That can be an indication of dynamical changes, i.e. alternation of the residual circulation between the equator and polar regions (for details, please see the discussion). Aside from the radiative forcing by direct or ozone heating, other factors are linked to the anomalies in the upper levels of the middle atmosphere (Haigh, 1994; Gray et al., 2009). It is necessary to take into consideration the dynamical coupling with the mesosphere through changes of the residual circulation (see below dynamical effects discussion). That can be illustrated by the positive anomaly around the stratopause in February (up to 4°C around 0.5 hPa). This anomaly propagates downward and together with spring radiative forcing affects the equatorial stratopause stability. Hemispheric asymmetry in the temperature response above the stratopause probably originates from the hemispheric differences, i.e. different wave activity. These statistically significant and positive temperature anomalies across the subtropical stratopause begin to descend and move to higher latitudes in the beginning of the northern winter. The anomalies manifest fully in February in the region between $60^\circ - 90^\circ$N and below 10 hPa and reach tropospheric levels - contrary to the results for the southern hemisphere. The southern hemispheric temperature anomaly is persistent above the stratopause and the solar cycle influence on the vortex stability differs from those in the northern hemisphere.

The above described monthly anomalies of the temperature correspond with the zonal wind anomalies throughout the year (Figs. 4 and 5(e)-(h)). Strengthening of the subtropical jets around the stratopause is the most apparent during winter in both hemispheres. This positive zonal wind anomaly gradually descends and moves poleward similar to (Frame and Gray, 2010) analysis based on ERA-40 data. In February, the intensive stratospheric warming and mesospheric cooling is associated with more pronounced transition from winter to summer circulation attributed to the solar cycle (in relative impact methodology up to 30%). In the southern hemisphere, this poleward motion of the positive zonal wind anomaly halts approximately at 60°S. For example in August, we can observe well-marked latitudinal zonal wind gradient (Fig. 4(g)). Positive anomalies in the geopotential height field correspond with the easterly zonal wind anomalies. The polar circulation reversal is associated with intrusion of the ozone from the lower latitudes as it is apparent, e.g., in August in the southern and in February in the northern hemisphere (last rows of Figs. 4 and 5).

In comparison with between the results of the MERRA and ERA-40 series studied by (Frame and Gray, 2010) There were found a distinct differences in October and November (Figs. 4(e)-(f)) in the equatorial region of the lower mesosphere. While in the MERRA reanalysis we have detected an easterly anomaly above 1 hPa in both months, westerly anomaly was identified in the ERA-40 series. Another distinct differences in the zonal mean temperature and zonal wind anomalies were not found.

5 Dynamical effects discussion

In this section, we discuss a dynamical impact of the solar cycle and its influence on the middle atmospheric winter conditions. The linear regression was applied on the EP diagnostics. Kodera and Kuroda (2002) suggested that the solar signal produced in the upper stratosphere region is transmitted to the lower stratosphere through modulation of the internal mode of variation in the polar night jet and through a change in the Brewer-Dobson circulation (prominent in the equatorial region in the lower stratosphere). In our analysis, we discussed the evolution of the winter circulation with an emphasis on the vortex itself rather than the behaviour of the jets. Further, we try to deduce possible processes leading to the observed differences in quantities of state between the solar maximum and minimum period. Because the superposition principle holds only for the linear processes, it is impossible to deduce the dynamics merely from the fields of differences. As noted by Kodera and Kuroda (2002), the dynamical response of the winter stratosphere includes highly nonlinear processes, e.g. wave mean flow interactions. Thus, both the anomaly and the total fields including climatology must be taken into account.

We start the analysis of the solar maximum dynamics with the period of the northern hemispheric winter circulation formation. The anomalies of the ozone, temperature, geopotential and Elliassen-Palm flux divergence support the hypothesis of weaker BDC during the solar maximum due to the less intensive wave pumping. This is consistent with previous studies (Kodera and Kuroda, 2002; Matthes et al., 2006). The causality is unclear, but the effect is visible in both branches of BDC as is explained on the basis of Fig. 4 and summarized schematically in Fig. 6.

During the early NH winter (including November) when westerlies are developed in the stratosphere, we can observe deeper polar vortex and consequent stronger westerly winds both inside and outside of the vortex. However, only the westerly anomaly outside the polar region and around 30°N from 10 hPa higher to the lower mesosphere is statistically significant (see the evolution of zonal wind anomalies in Figs. 4(e)-(h)). The slightly different wind field has a direct influence on the vertical propagation of planetary waves.

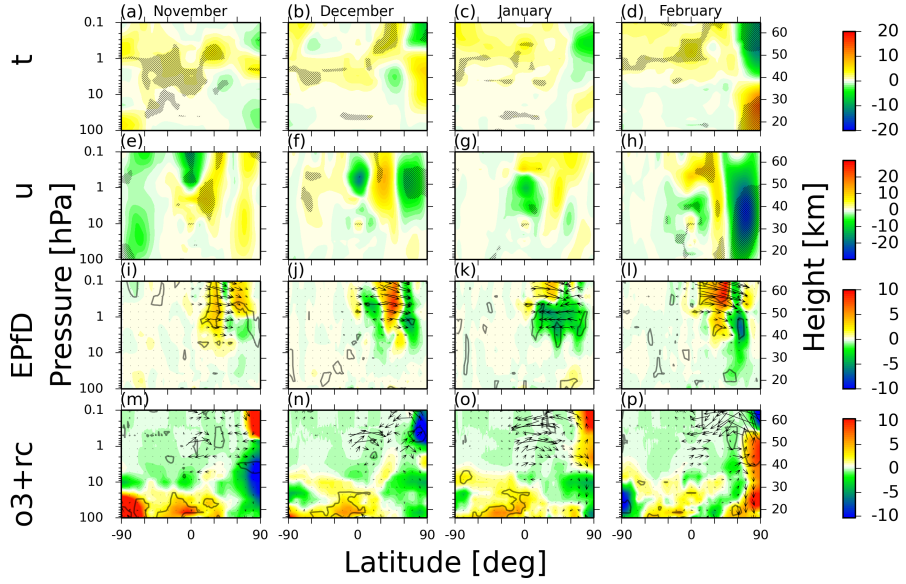

Figure 4. The monthly averaged response of solar signal in the MERRA zonal-mean temperature t (a)-(d), unit: $[^{\circ}\mathrm{C}]$; zonal wind u (e)-(h), unit: $[\mathrm{m/s}]$; EP flux divergence $EPfD$ (i)-(l), unit: $[\mathrm{m/s/day}]$; together with EP flux vectors scaled by the inverse of the pressure, unit: $[\mathrm{kg/s^2}]$; and ozone mixing ratio, unit: percentage change per monthly mean; with residual circulation $o3 + rc$ (m)-(p), units: $[\mathrm{m/s;m/s}]$ during northern hemispheric winter. The response is expressed as regression coefficients (corresponding units per S_{max} minus S_{min}). Statistical significance of scalar fields was computed by t-test. Hatches in Figs. (a)-(h) and grey contours in Figs. (i)-(p) indicate p-values $<$ 0.05 respectively.

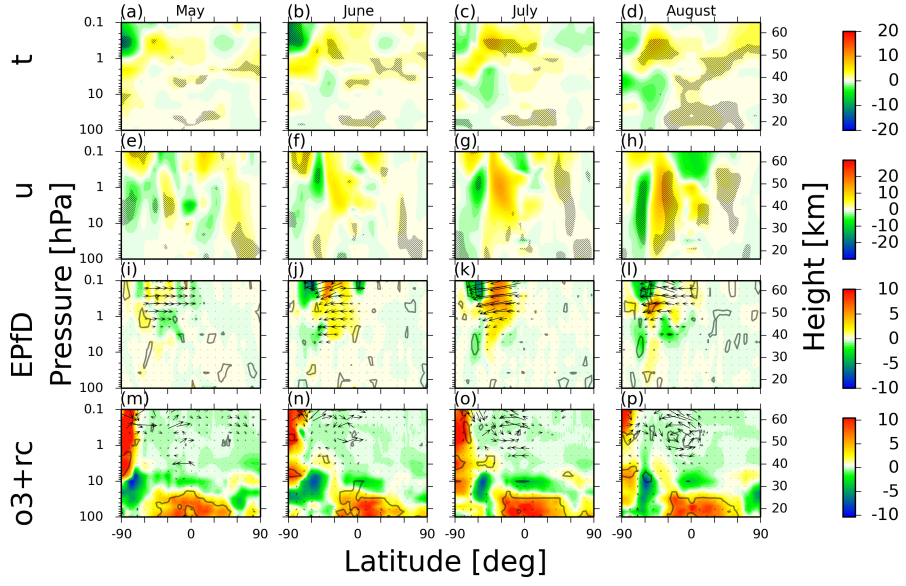

Figure 5. The monthly averaged response of solar signal in the MERRA zonal-mean temperature t (a)-(d), unit: $[^{\circ}\mathrm{C}]$; zonal wind u (e)-(h), unit: $[\mathrm{m/s}]$; EP flux divergence $EPfD$ (i)-(l), unit: $[\mathrm{m/s/day}]$; together with EP flux vectors scaled by the inverse of the pressure, unit: $[\mathrm{kg/s^2}]$; and ozone mixing ratio, unit: percentage change per monthly mean; with residual circulation $o3 + rc$ (m)-(p), units: $[\mathrm{m/s;Pa/s}]$ during southern hemispheric winter. The response is expressed as regression coefficients (corresponding units per S_{max} minus S_{min}). Statistical significance of scalar fields was computed by t-test. Hatches in Figs. (a)-(h) and grey contours in Figs. (i)-(p) indicate p-values $<$ 0.05 respectively

From the Elliassen-Palm flux anomalies and climatology we can see that the waves propagate vertically with increasing

poleward instead of equatorward meridional direction with height. This is then reflected in the EP flux divergence field, where the region of maximal convergence is shifted poleward and the anomalous convergence region emerges inside the vortex above approximately 50 hPa (Figs. 4(i)-(l)).

The poleward shift of the maximum convergence area further contributes to the reduced BDC. This is again confirmed by the temperature and ozone anomalies. The anomalous convergence inside the vortex induces anomalous residual circulation, the manifestation of which is clearly seen in the quadrupole-like temperature structure (positive and negative anomalies are depicted schematically in Fig. 6 using red and blue boxes respectively). This pattern emerges in November and even more clearly in December. In December, the induced residual circulation leads to an intrusion of the ozone rich air into the vortex at about 1 hPa level (Fig. 4(o)). The inhomogeneity in the vertical structure of the vortex is then pronounced also in the geopotential height differences. That corresponds with the temperature analysis in the sense that above and in the region of colder anomaly there is a negative geopotential anomaly and vice versa. The geopotential height difference has a direct influence on the zonal wind field (via thermal wind balance). The result is a deceleration of the upper vortex parts and consequent broadening of the upper parts (due to conservation of angular momentum).

Considering the zonal wind field, the vortex enters January having approximately its average climatological extent. The wind speeds in its upper parts are slightly higher. That is because of the smaller geopotential values corresponding with the negative temperature anomalies above approximately 1 hPa. This results from the absence of adiabatic heating due to the suppressed BDC, although the differences in quantities of state (temperature and geopotential height) are small and insignificant (see the temperature anomalies in Fig. 4(c)). It is important to note that these differences change sign around 40 km altitude inside the vortex further accentuating the vertical inhomogeneity of the vortex. This might start balancing processes inside the vortex, which is confirmed by analysis of the dynamical quantities, i.e. EP flux and its divergence (Fig. 4(k)). Detailed description of these processes is the key in understanding the dynamics and causality of Sudden Stratospheric Warmings (SSW) taking place in February.

Significant anomalies of the EP flux indicate anomalous vertical wave propagation resulting in the strong anomalous EP flux convergence significantly pronounced in a horizontally broad region and confined to upper levels (convergence (negative values) drawn by green or blue shades in Figs. 4(i)-(l)). This leads to induction of an anomalous residual circulation starting to gain intensity in January. The situation then results in disruption of the polar vortex visible in February in significant anomalies of quantities of state - in contrast to January. Further strong mixing of air is suggested by the ozone fields. The quadrupole-like structure of the temperature is visible across the whole NH middle atmosphere in February (indicated in the lower diagram of Fig. 6). Especially in the higher latitudes, this is very significant and well pronounced by the stratospheric warming and mesospheric cooling.

The hemispheric asymmetry of the solar cycle influence can be documented especially on the winter conditions as was already suggested in the Section 4.2. Since the positive zonal wind anomaly halts approximately at 60°S and intensifies over 10 m/s, one would expect the poleward deflection of the planetary waves propagation according to NH winter mechanisms discussed above. This is actually observed in June to August when the highest negative anomalies of the latitudinal coordinates of EP flux are located in the upper stratosphere and above in the lower mesosphere (Figs. 5(j)-(l)). Anomalous divergence of EP flux is developed around the stratopause between 30°S and 60°S. Similarly to the hypothetical mechanism of weaker BDC described above, we can observe less wave pumping in the stratosphere and consequently assume less upwelling in the equatorial region. However, the anomalies of the residual circulation pointing to the weaker BDC are not so well established as in the case of NH winter. These mechanisms could lead to a explanation of the more pronounced temperature response to the solar signal in the equatorial region of the lower stratosphere in August in the SH winter (above 1°C) than in December in the NH winter (around 0.5°C). This is in agreement with another observational study (van Loon and Labitzke, 2000). Overall, the lower stratospheric temperature anomaly is more coherent in the SH winter than in the NH winter, where the solar signal is not so well apparent and statistically significant in particular months and reanalysis datasets.

6 Conclusions

We have analyzed the changes of the air temperature, ozone and circulation characteristics driven by the variability of the eleven years solar cycle influence in the stratosphere and lower mesosphere. The attribution analysis was performed on the last generation of reanalyzed data, and was aimed to compare how this type of datasets resolves the solar variability throughout the levels where the "top-down" mechanism is assumed. Furthermore, the results originated in the linear attribution using MLR were compared with other relevant observational studies and supported by the nonlinear attribution analysis using SVR and MLP techniques.

The solar signal extracted from the temperature field from MERRA and ERA-Interim reanalysis using the linear regression has the amplitudes around 1°C and 0.5°C, in the upper stratospheric and in the lower stratospheric equatorial region, respectively. These signals, statistically significant at p-value < 0.01, can be considered sufficiently robust and they are in qualitative agreement with previous observational studies (e.g. Frame and Gray, 2010)) since we have used the last generation of reanalyzed datasets extended to 2013. The statistically significant signal was observed only in the lower

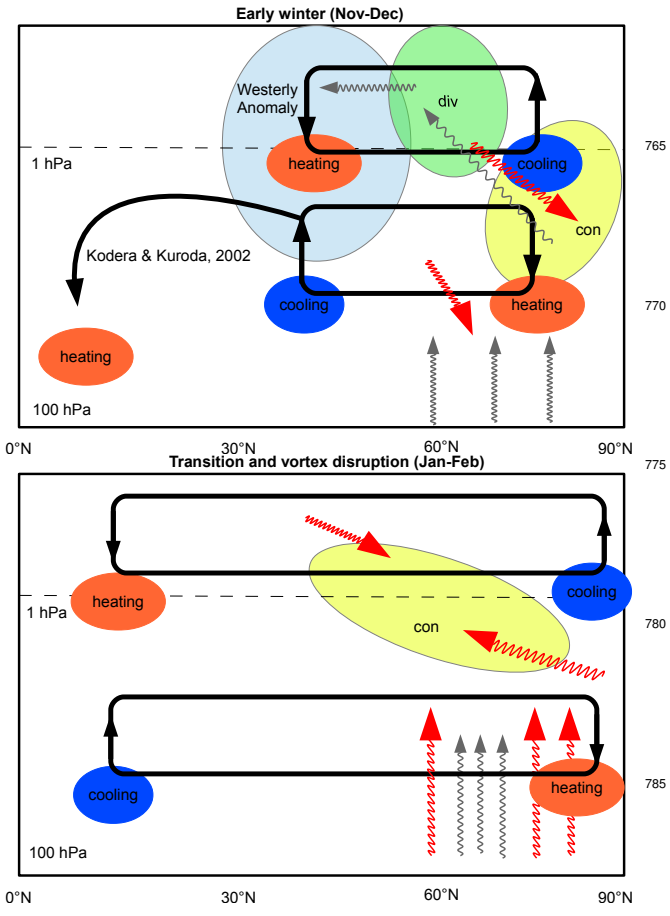

Figure 6. Solar cycle modulation of the winter circulation: schema of the related mechanisms. The upper and lower figure show early and later winter respectively. The anomaly heating and cooling are drawn by red and blue boxes. The EP flux divergence and convergence are drawn by green and yellow boxes. The anomaly wave propagation is expressed as wavy red arrow in contrast to the climatological average drawn by wavy grey arrow. The induced residual circulation according to quasi-geostrophic approximation is highlighted by the bold black lines.

part of the stratosphere in the JRA-55 reanalysis, however with similar amplitudes as in the other datasets.

Similar to the temperature response, the double-peaked solar response in the ozone was detected in the satellite measurements (e.g. Soukharev and Hood, 2006) and even confirmed by the coupled chemistry climate model simulations (e.g. **?**). However, the exact position and amplitude of both ozone anomalies remains a point of disagreement between models and observations. The results of our attribution analysis point to large differences in the upper stratospheric ozone response to the solar cycle in comparison with the studies mentioned above and even between reanalyses themselves. The upper stratospheric ozone reaches 2% in the SBUV(/2) satellite measurements (e.g. Soukharev and Hood, 2006, Fig. 5), which were assimilated as the only source of ozone profiles into MERRA reanalysis. This fact is remarkable since the same signal was not detected in the upper stratosphere in the MERRA results. However, the solar signal in the ozone field seems to be shifted above the stratopause where similar and statistically significant solar variability was attributed. Concerning the solar signal in the ERA-Interim, there is a negative ozone response via regression coefficient in the upper stratosphere although the solar variability expressed as relative impact appears to be in agreement with satellite measurements. Furthermore, the lower stratospheric solar response in the ERA-Interim's ozone is reduced in this dataset around the equator and shifted to higher latitudes. Another difference was detected in the monthly response of the zonal wind in October and November in the equatorial region of the lower mesosphere between the results for the MERRA series and ERA-40 data studied by Frame and Gray (2010). While in the MERRA reanalysis we have detected the easterly anomaly, westerly anomaly was identified in the ERA-40 series.

Similar problem with the correct resolving of the double-peaked ozone anomaly was registered in study of Dhomse et al. (2011) which investigated the solar response in the tropical stratospheric ozone using 3D chemical transport model. The upper stratospheric solar signal observed in SBUV/SAGE and SAGE-based data could be reproduced only in model runs with unrealistic dynamics, i.e. with no inter-annual meteorological changes.

The nonlinear approach to attribution analysis, represented by application of the SVR and MLP, largely confirmed the solar response computed by the linear regression. Consequently, these results can be considered quite robust regarding the statistical modelling of the solar variability in the middle atmosphere. This finding indicates that the linear regression is a technique sufficient to resolve the basic shape of the solar signal through the middle atmosphere. However, some uncertainties could partially stem from the fact that the SVR and MLP techniques are highly dependent on optimal model setting that requires rigorous crossvalidation process (which places high demands on computing time). As a benefit, the nonlinear techniques show an ability to simulate the middle atmosphere variability with higher accuracy than the linear regression.

In the dynamical effects discussion, we described dynamical impact of the solar cycle on the middle atmospheric winter conditions. Main part deals with the solar influence on the northern winter conditions, nevertheless the southern winter anomalies were also discussed. The relevant dynamical effects are summarized in schematic diagrams (Fig. 6). Both diagrams depict average conditions and anomalies induced by the solar cycle. The first one summarizes how equatorward wave propagation is influenced by the westerly anomaly around subtropical stratopause. The quadrupole-like temperature structure is explained by anomalous residual circulation in the higher latitudes together with the anomalous branch heading towards the equatorial region hypothe-

sized already by Kodera and Kuroda (2002). The second diagram concludes transition time to vortex disruption during February. Again very apparent quadrupole-like structure of the temperature is even more pronounced especially in the polar region and seems to be more extended to lower latitudes. However, we can strongly assume that the dynamical effects are not zonally uniform, as it is supposed and presented here using two-dimensional (2D) EP diagnostics and TEM equations. So it would be desirable to extend the discussion of dynamical effects by other relevant characteristics for example by analysis of wave propagation and wave-mean flow interaction using the 3D formulation (Kinoshita and Sato, 2013).

This paper is fully focused on the solar cycle influence, i.e. on decadal changes in the stratosphere and lower mesosphere, although huge amount of results concerning other forcings was generated by the attribution analysis. The QBO phenomenon can be one of them since the solar-QBO interaction and the modulation of Holtan-Tan relationship by the solar cycle are regarded as highly challenging, especially in the global climate simulations (Matthes et al., 2013).

Acknowledgements. The authors thank to the relevant working teams for the reanalysis datasets: MERRA (obtained from NASA, http://disc.sci.gsfc.nasa.gov/daac-bin/DataHoldings.pl), ERA-Interim (obtained from ECMWF, http://apps.ecmwf.int/datasets/) and JRA-55 (obtained from http://jra.kishou.go.jp/JRA-55/index_en.html). The study was supported by the Charles University in Prague, Grant Agency project No. 1474314, and by the grant No. SVV-2014-26096.

References

Andrews, D. G. and McIntyre, M. E.: JR Holton, and CB Leovy, 1987: Middle Atmosphere Dynamics, 1987.

Baldwin, M. P. and Dunkerton, T. J.: Propagation of the Arctic Oscillation from the stratosphere to the troposphere, Journal of Geophysical Research: Atmospheres (1984–2012), 104, 30 937–30 946, 1999.

Blume, C. and Matthes, K.: Understanding and forecasting polar stratospheric variability with statistical models, Atmos. Chem. Phys, 12, 5691–5701, 2012.

Camp, C. D. and Tung, K.: The influence of the solar cycle and QBO on the late-winter stratospheric polar vortex, Journal of the atmospheric sciences, 64, 1267–1283, 2007.

Cortes, C. and Vapnik, V.: Support-vector networks, Machine Learning, 20, 273–297, doi:10.1007/BF00994018, http://link.springer.com/10.1007/BF00994018, 1995.

Coughlin, K. and Tung, K.-K.: Eleven-year solar cycle signal throughout the lower atmosphere, Journal of Geophysical Research: Atmospheres (1984–2012), 109, 2004.

Crooks, S. A. and Gray, L. J.: Characterization of the 11-year solar signal using a multiple regression analysis of the ERA-40 dataset, Journal of climate, 18, 996–1015, 2005.

Dee, D., Uppala, S., Simmons, A., Berrisford, P., Poli, P., Kobayashi, S., Andrae, U., Balmaseda, M., Balsamo, G., Bauer, P., et al.: The ERA-Interim reanalysis: Configuration and performance of the data assimilation system, Quarterly Journal of the Royal Meteorological Society, 137, 553–597, 2011.

Dhomse, S., Chipperfield, M. P., Feng, W., and Haigh, J. D.: Solar response in tropical stratospheric ozone: a 3-D chemical transport model study using ERA reanalyses, Atmospheric Chemistry and Physics, 11, 12 773–12 786, doi:10.5194/acp-11-12773-2011, http://www.atmos-chem-phys.net/11/12773/2011/, 2011.

Ebita, A., Kobayashi, S., Ota, Y., Moriya, M., Kumabe, R., Onogi, K., Harada, Y., Yasui, S., Miyaoka, K., Takahashi, K., et al.: The Japanese 55-year Reanalysis (JRA-55): an interim report, Sola, 7, 149–152, 2011.

Edmon Jr, H., Hoskins, B., and McIntyre, M.: Eliassen-Palm cross sections for the troposphere, Journal of the Atmospheric Sciences, 37, 2600–2616, 1980.

Frame, T. H. A. and Gray, L. J.: The 11-Yr Solar Cycle in ERA-40 Data: An Update to 2008, Journal of Climate, 2010.

Fujiwara, M., Polavarapu, S., and Jackson, D.: A proposal of the SPARC reanalysis/analysis intercomparison project, SPARC Newsletter, 38, 14–17, 2012.

Gerber, E. P., Butler, A., Calvo, N., Charlton-Perez, A., Giorgetta, M., Manzini, E., Perlwitz, J., Polvani, L. M., Sassi, F., Scaife, A. A., et al.: Assessing and Understanding the Impact of Stratospheric Dynamics and Variability on the Earth System., Bulletin of the American Meteorological Society, 93, 2012.

Gevrey, M., Dimopoulos, I., and Lek, S.: Review and comparison of methods to study the contribution of variables in artificial neural network models, Ecological Modelling, 160, 249–264, 2003.

Gray, L. J., Crooks, S., Pascoe, C., Sparrow, S., and Palmer, M.: Solar and QBO influences on the timing of stratospheric sudden warmings, Journal of the atmospheric sciences, 61, 2777–2796, 2004.

Gray, L. J., Rumbold, S., and Shine, K. P.: Stratospheric temperature and radiative forcing response to 11-year solar cycle changes in irradiance and ozone, Journal of the Atmospheric Sciences, 66, 2402–2417, 2009.

Gray, L. J., Beer, J., Geller, M., Haigh, J. D., Lockwood, M., Matthes, K., Cubasch, U., Fleitmann, D., Harrison, G., Hood, L., et al.: Solar influences on climate, Reviews of Geophysics, 48, RG4001, 2010.

Gray, L. J., Scaife, A. A., Mitchell, D. M., Osprey, S., Ineson, S., Hardiman, S., Butchart, N., Knight, J., Sutton, R., and Kodera, K.: A lagged response to the 11 year solar cycle in observed winter Atlantic/European weather patterns, Journal of Geophysical Research: Atmospheres, 118, 13,405–13,420, doi:10.1002/2013JD020062, http://dx.doi.org/10.1002/2013JD020062, 2013.

Haigh, J. D.: The role of stratospheric ozone in modulating the solar radiative forcing of climate, Nature, 370, 544–546, 1994.

Harder, J. W., Fontenla, J. M., Pilewskie, P., Richard, E. C., and Woods, T. N.: Trends in solar spectral irradiance variability in the visible and infrared, Geophysical Research Letters, 36, 2009.

Haykin, S. S., Haykin, S. S., Haykin, S. S., and Haykin, S. S.: Neural networks and learning machines, vol. 3, Pearson Education Upper Saddle River, 2009.

Holton, J. R. and Tan, H.-C.: The influence of the equatorial quasi-biennial oscillation on the global circulation at 50 mb, Journal of the Atmospheric Sciences, 37, 2200–2208, 1980.

Hood, L., Schimanke, S., Spangehl, T., Bal, S., and Cubasch, U.: The Surface Climate Response to 11-Yr Solar Forcing during Northern Winter: Observational Analyses and Comparisons with GCM Simulations, Journal of Climate, 26, 7489–7506, doi:10.1175/JCLI-D-12-00843.1, http://dx.doi.org/10.1175/JCLI-D-12-00843.1, 2013.

Hood, L. L. and Soukharev, B. E.: The Lower-Stratospheric Response to 11-Yr Solar Forcing: Coupling to the Troposphere-Ocean Response, Journal of the Atmospheric Sciences, 69, 1841–1864, doi:10.1175/JAS-D-11-086.1, http://dx.doi.org/10.1175/JAS-D-11-086.1, 2012.

Hood, L. L., Soukharev, B. E., and McCormack, J. P.: Decadal variability of the tropical stratosphere: Secondary influence of the El Niño–Southern Oscillation, Journal of Geophysical Research, 115, D11 113, 2010.

Ineson, S., Scaife, A. A., Knight, J. R., Manners, J. C., Dunstone, N. J., Gray, L. J., and Haigh, J. D.: Solar forcing of winter climate variability in the Northern Hemisphere, Nature Geoscience, 4, 753–757, 2011.

Kinoshita, T. and Sato, K.: A formulation of unified three-dimensional wave activity flux of inertia–gravity waves and Rossby waves, Journal of the Atmospheric Sciences, 70, 1603–1615, 2013.

Kodera, K. and Kuroda, Y.: Dynamical response to the solar cycle, Journal of Geophysical Research: Atmospheres, 107, ACL 5–1–ACL 5–12, doi:10.1029/2002JD002224, http://dx.doi.org/10.1029/2002JD002224, 2002.

Kohavi, R. et al.: A study of cross-validation and bootstrap for accuracy estimation and model selection, in: IJCAI, vol. 14, pp. 1137–1145, 1995.

Labitzke, K.: Sunspots, the QBO, and the stratospheric temperature in the north polar region, Geophysical Research Letters, 14, 535–537, doi:10.1029/GL014i005p00535, http://dx.doi.org/10.1029/GL014i005p00535, 1987.

Labitzke, K., Kunze, M., and Bronnimann, S.: Sunspots, the QBO and the stratosphere in the North Polar Region 20 years later, Meteorologische Zeitschrift, 15, 355–363, 2006.

Lean, J.: Short term, direct indices of solar variability, Solar Variability and Climate, pp. 39–51, 2001.

Lu, H., Franzke, C., Martius, O., Jarvis, M. J., and Phillips, T.: Solar wind dynamic pressure effect on planetary wave propagation and synoptic-scale Rossby wave breaking, Journal of Geophysical Research: Atmospheres, 118, 4476–4493, 2013.

Matthes, K., Kuroda, Y., Kodera, K., and Langematz, U.: Transfer of the solar signal from the stratosphere to the troposphere: Northern winter, Journal of geophysical research, 111, D06 108, 2006.

Matthes, K., Kodera, K., Garcia, R. R., Kuroda, Y., Marsh, D. R., and Labitzke, K.: The importance of time-varying forcing for QBO modulation of the atmospheric 11 year solar cycle signal, Journal of Geophysical Research: Atmospheres, 118, 4435–4447, doi:10.1002/jgrd.50424, http://doi.wiley.com/10.1002/jgrd.50424, 2013.

McLandress, C., Plummer, D., and Shepherd, T.: Technical Note: A simple procedure for removing temporal discontinuities in ERA-Interim upper stratospheric temperatures for use in nudged chemistry-climate model simulations, Atmospheric Chemistry and Physics Discussions, 13, 25 801–25 825, 2013.

NCAR: The Climate Data Guide: Multivariate ENSO Index, Retrieved from https://climatedataguide.ucar.edu/climate-data/multivariate-enso-index, last modified 20 Aug 2013, 2013.

Neter, J., Kutner, M., Wasserman, W., and Nachtsheim, C.: Applied Linear Statistical Models, McGraw-Hill/Irwin, 2004.

NWS: Northern Atlantic Oscillation index, Retrieved from http://www.cpc.ncep.noaa.gov/products/precip/CWlink/pna/nao.shtml, last modified daily, 2013.

Olden, J. D. and Jackson, D. A.: Illuminating the "black box": a randomization approach for understanding variable contributions in artificial neural networks, Ecological Modelling, 154, 135–150, doi:10.1016/S0304-3800(02)00064-9, http://linkinghub.elsevier.com/retrieve/pii/S0304380002000649, 2002.

Pasini, A., Lorè, M., and Ameli, F.: Neural network modelling for the analysis of forcings/temperatures relationships at different scales in the climate system, Ecological Modelling, 191, 58–67, doi:10.1016/j.ecolmodel.2005.08.012, http://linkinghub.elsevier.com/retrieve/pii/S0304380005003492, 2006.

Pisoft, P., Holtanova, E., Huszar, P., Miksovsky, J., and Zak, M.: Imprint of the 11-year solar cycle in reanalyzed and radiosonde datasets: a spatial frequency analysis approach, Climatic Change, 110, 85–99, doi:10.1007/s10584-011-0147-0, http://dx.doi.org/10.1007/s10584-011-0147-0, 2012.

Pisoft, P., Holtanova, E., Huszar, P., Kalvova, J., Miksovsky, J., Raidl, A., Zemankova, K., and Zak, M.: Manifestation of reanalyzed QBO and SSC signals, Theoretical and Applied Climatology, pp. 1–10, 2013.

Randel, W. J. and Wu, F.: A stratospheric ozone profile data set for 1979–2005: Variability, trends, and comparisons with column ozone data, Journal of Geophysical Research: Atmospheres (1984–2012), 112, 2007.

Rienecker, M. M., Suarez, M. J., Gelaro, R., Todling, R., Bacmeister, J., Liu, E., Bosilovich, M. G., Schubert, S. D., Takacs, L., Kim, G. K., et al.: MERRA: NASA's modern-era retrospective analysis for research and applications, Journal of Climate, 24, 3624–3648, 2011.

Sato, M., Hansen, J. E., McCormick, M. P., and Pollack, J. B.: Stratospheric aerosol optical depths, 1850-1990, Journal of Geophysical Research: Atmospheres, 98, 22 987–22 994, doi:10.1029/93JD02553, http://dx.doi.org/10.1029/93JD02553, 1993.

Solomon, S., Rosenlof, K. H., Portmann, R. W., Daniel, J. S., Davis, S. M., Sanford, T. J., and Plattner, G.-K.: Contributions of stratospheric water vapor to decadal changes in the rate of global warming, Science, 327, 1219–1223, 2010.

Soukharev, B. E. and Hood, L. L.: Solar cycle variation of stratospheric ozone: Multiple regression analysis of long-term satellite data sets and comparisons with models, Journal of Geophysical Research: Atmospheres, 111, 20 314, 2006.

Thejll, P.and Schmith, T.: Limitations on regression analysis due to serially correlated residuals: Application to climate reconstruction from proxies, Journal of geophysical research, 110, D18 103, 2005.

van Loon, H. and Labitzke, K.: The Influence of the 11-year Solar Cycle on the Stratosphere Below 30 km: a Review, Space Science Reviews, 94, 259–278, doi:10.1023/A:1026731625713, http://dx.doi.org/10.1023/A%3A1026731625713, 2000.

van Loon, H. and Meehl, G. A.: The response in the Pacific to the Sun's decadal peaks and contrasts to cold events in the South-

ern Oscillation, Journal of Atmospheric and Solar-Terrestrial Physics, 70, 1046–1055, 2008.

van Loon, H., Meehl, G., and Shea, D.: The effect of the decadal solar oscillation in the Pacific troposphere in northern winter, J. Geophys. Res, 112, D02 108, 2007.

Walter, A. and Schönwiese, C. D.: Nonlinear statistical attribution and detection of anthropogenic climate change using a simulated annealing algorithm, Theoretical and Applied Climatology, 76, 1–12, doi:10.1007/s00704-003-0008-5, http://link.springer.com/10.1007/s00704-003-0008-5, 2003.